Anticancer Therapeutics

Deutsche Ausgabe: DOI: 10.1002/ange.201600753
Internationale Ausgabe: DOI: 10.1002/anie.201600753

Regulating the Rate of Molecular Self-Assembly for Targeting Cancer Cells

*Jie Zhou, Xuewen Du, and Bing Xu**

Abstract: *Besides tight and specific ligand–receptor interactions, the rate regulation of the formation of molecular assemblies is one of fundamental features of cells. But the latter receives little exploration for developing anticancer therapeutics. Here we show that a simple molecular design of the substrates of phosphatases—tailoring the number of phosphates on peptidic substrates—is able to regulate the rate of molecular self-assembly of the enzyme reaction product. Such a rate regulation allows selective inhibition of osteosarcoma cells over hepatocytes, which promises to target cancer cells in a specific organ. Moreover, our result reveals that the direct measurement of the rate of the self-assembly in a cell-based assay provides precise assessment of the cell targeting capability of self-assembly. This work, as the first report establishing rate regulation of a multiple-step process to inhibit cells selectively, illustrates a fundamentally new approach for controlling the fate of cells.*

This study reports targeting cancer cells by the control of the rate of the formation of supramolecular assemblies. Molecular-targeted therapeutics, which mostly relies on tight ligand–receptor interaction or enzyme inhibition, has been a key strategy for developing cancer drugs. However, recent advances in cancer biology have revealed the great complexity of cancers, such as redundant signaling pathways, adaptive drug resistance, genomic instability, intratumoral heterogeneity, and tumor microenvironment.[1] These conceptual advances not only elucidate that the major root of drug resistance in current cancer therapy is the reliance on specific, tight ligand–receptor binding of only one or two molecular targets (e.g., enzymes, receptors, or transcription factors), but also underscore an urgent need of new approaches for cancer therapy. Recognizing that cancer immunotherapy essentially is a form of spatiotemporal controlled apoptosis in human body and enzyme-instructed self-assembly (EISA) is an inherent feature of apoptosis,[2] we have departed from the dogma of specific ligand–receptor binding and are focusing on integrating enzyme transformation (ET) and self-assembly (SA)[3] to generate the fibrils of small molecules as potential anticancer therapeutics.[4]

Based on the development of enzymatic self-assembly and hydrogelation/aggregation of small molecules,[5] we have employed alkaline phosphatases (ALP) to catalyse the formation of nanofibrils of small peptidic hydrogelators in pericellular space of cancer cells, thus achieved selective inhibition of cancer cells, including drug-resistant ones.[4c] This approach turns out to be general since the use of a phosphorylated carbohydrate[6] or phosphorylated nanoparticles[7] as the substrates of ALP for EISA also selectively inhibit cancer cells. These results, undoubtedly, establish that EISA is able to utilize "undruggable" enzymes, such as ALP,[8] for generating molecular nanofibrils to inhibit cancer cells. Despite the promises of the ALP-based EISA for potential cancer therapy, the ubiquitous presence of ALPs in human body presents a unique challenge. As revealed by the studies of mammalian ALPs,[9] being a type of ectoenzymes and present in all tissues throughout the entire body for important biological functions, ALPs exist in four typical isozymes—placental alkaline phosphatase (ALPP), germ cell alkaline phosphatase (ALPP2), intestinal alkaline phosphatase (ALPI), and tissue non-specific alkaline phosphatase (ALPL). Although ALPP overexpresses only on certain cancer cells and not on normal cells, ALPL expresses on normal cells.[10] While the apparent solution for selectivity is to develop a substrate being dephosphorylated by ALPP only, it would not be an easy task for two reasons. First, the inability to develop a highly selective inhibitor for ALPP over ALPL implies that ALPP and ALPL are indiscriminate to their substrates. Second, there is little structural information of ALPL, which makes the design of specific substrates difficult, if not impossible. In addition, a single cell can co-express different isozymes of ALP, albeit at different levels, further complicating the situation. These facts demand a new strategy for precisely targeting cancer cells in a desired organ or tissue, particularly in the case of cancer cells overexpressing ALPL.

To meet the above need, we choose to use the rate of molecular self-assembly to amplify the difference of the expression level of ALPs in cancer and normal cells for targeting cancer cells. As a demonstration of concept, we select two cell lines (i.e., HepG2 (liver hepatocellular carcinoma) and Saos-2 (osteosarcoma)) known to express ALPL and design two kinds of substrates (i.e., monophosphorylated and diphosphorylated peptides, Figure 1) of ALPL for regulating the rate of self-assembly. We choose HepG2 and Saos-2 because the former acts as the model cell of hepatocytes[11] and the latter is known to overexpress ALPL on membrane.[6] Our antibody staining reveals that HepG2 cells, indeed, express less ALPLs than Saos-2 does. Tailoring the rate of self-assembly is able to amplify such a subtle difference in the expression of ALPL. As illustrated in Scheme 1, the rate for generating the self-assembling peptide (i.e., **TPD**) should be slower from the diphosphorylated substrates (i.e., **TPD-2p**) than from the monophos-

[*] J. Zhou, X. W. Du, Prof. Dr. B. Xu
Department of Chemistry, Brandeis University
415 South St, Waltham, MA 02454 (USA)
E-mail: bxu@brandeis.edu

Supporting information for this article can be found under: http://dx.doi.org/10.1002/anie.201600753.

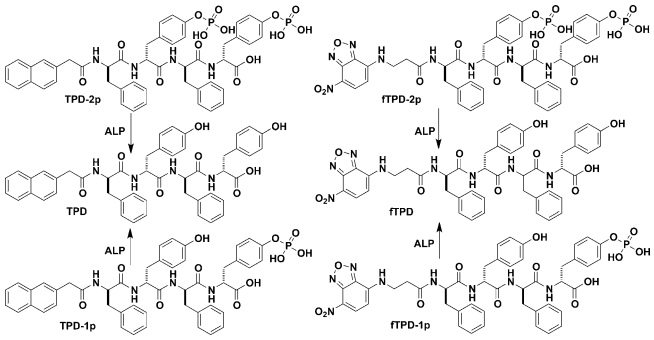

Figure 1. Molecular structures of the tetrapeptide derivatives/precursors with two or one phosphotyrosines (**TPD-2p** and **TPD-1p**) and their fluorescent analogs (**fTPD-2p** and **fTPD-1p**). These precursors turn into the self-assembling D-peptidic hydrogelators (i.e., **TPD** and **fTPD**) after enzymatic dephosphorylation by alkaline phosphatase (ALP).

phorylated substrates (i.e., **TPD-1p**) because the former requires dephosphorylation twice. Cell viability assays indicate that, while **TPD-2p** and **TPD-1p** exhibit similar inhibitory activities against Saos-2 cells, **TPD-2p** is more cell compatible than **TPD-1p** towards HepG2 cells. Moreover, the fluorescent analogues of **TPD-2p** and **TPD-1p** (i.e., **fTPD-2p** and **fTPD-1p**) confirm that the diphosphorylated substrate results in little molecular assemblies on HepG2 cells, but monophosphorylated substrate affords significant amount of molecular assemblies on HepG2 cells. These results establish that it is feasible to achieve excellent targeting selectivity by using the rate of molecular self-assembly to amplify the difference of ectoenzyme expressions on different cells/tissues. Besides being the first report of using rate regulation of a multiple-step process to inhibit cells selectively, this work illustrates a novel approach for developing therapeutics that may pass by liver and target the tumor site (e.g., sites of osteosarcoma) for selectively killing cancer cells.

We have validated that a small D-tripeptide derivative, Nap-D-Phe-D-Phe-D-$_p$Tyr, with the tyrosine phosphorylated, selectively inhibits cancer cells due to the different expression of ALPs between cancer (e.g., HeLa) and normal (e.g., HS-5) cells.[4c,d,10b] Based on this result and that aromatic ring of tyrosine promotes self-assembly,[4e] we design a D-tetrapeptide derivative (**TPD-1p**, Figure 1) by inserting a tyrosine between two phenylalanine residues of that D-tripeptide derivative. Besides potentially retaining or even enhancing the self-assembly ability of the D-tetrapeptide, the additional tyrosine residue provides another site for phosphorylation, which affords a diphosphorylated substrate (**TPD-2p**) for ALP. We expect the ALP-catalysed formation of **TPD** would be slower from **TPD-2p** than from **TPD-1P**. To directly visualize the self-assembly behaviour of **TPD** generated from these two types of precursors, we design **fTPD-2p** and **fTPD-1p** (Figure 1) as the fluorescent analogues of **TPD-2p** and **TPD-1p** by replacing the Nap motif with nitrobenzoxadiazole (NBD), a fluorophore known to fluoresce brightly in assembled state.[4e] After preparing the non-commercial starting materials (e.g., Fmoc-phosphotyrosine and NBD-COOH (Figure S1 in the Supporting Information, SI)) prior to solid phase peptide synthesis (SPPS),[12] we used SPPS for the synthesis and high-performance liquid chromatography (HPLC) for the purification and obtained the molecules shown in Figure 1 in good yields (60–80%). LC-MS and ^{1}H NMR confirm the purity and structures of these designed molecules (SI)

Both **TPD-2p** and **TPD-1p** dissolve well in water to make transparent solutions at physiological pH 7.4 at the concentration of 500 μM (the highest concentration used in cell experiment) (Figure S2A). The solubility of **TPD-2p** is better than that of **TPD-1p** due to an additional phosphate. Transmission electron microscopy (TEM) images of their solutions after water evaporation show that both **TPD-2p** and **TPD-1p** form few amorphous aggregates (Figure 2A), suggesting that the majorities are still oligomers or monomers that cannot be visualized by TEM. Having the same peptide backbone, either **TPD-2p** or **TPD-1p** results in the same self-assembling molecule **TPD** after its complete dephosphorylation catalyzed by ALP. This feature explains that treating the above solutions with ALP (1 U mL^{-1}) leads to the same viscous solutions (Figure S2A) with same nanofibrils ($d = 5 \pm 2$ nm) in them (Figure 2A). **TPD-2p** takes longer time to be completely dephosphorylated due to the second phosphate, as evidenced by that **TPD-2p** takes longer time (Figure S2B)

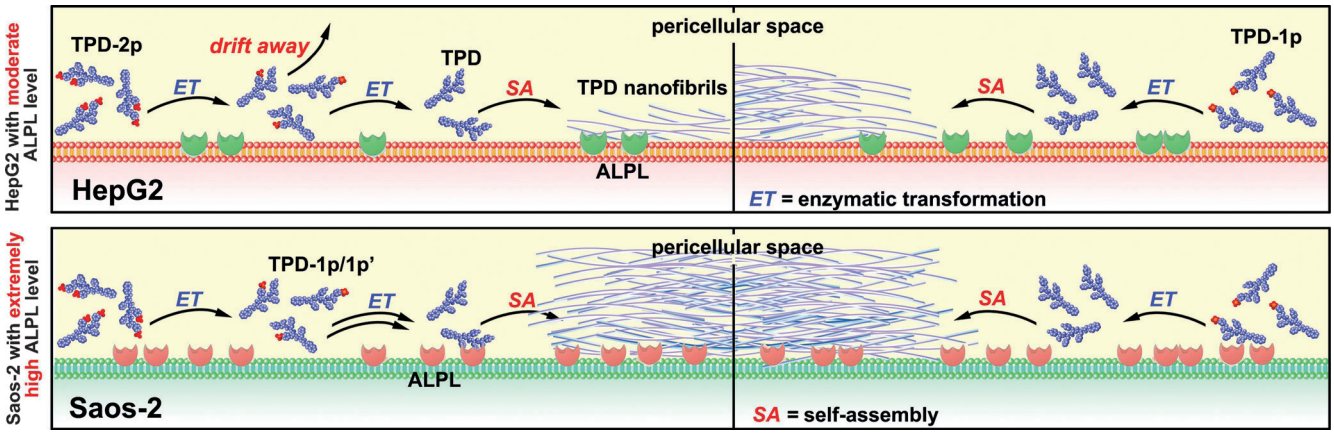

Scheme 1. Illustration of the use of the rate of molecular self-assembly (controlled by numbers of enzymatic site) to amplify the difference of the expression level of ALPs in different cell lines.

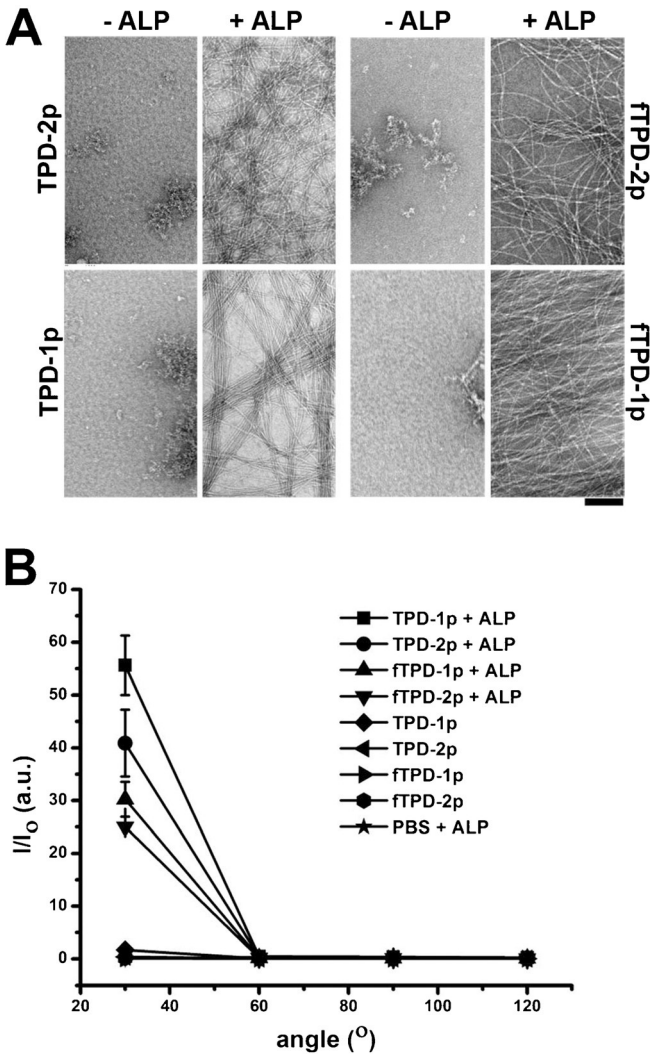

Figure 2. A) TEM images and B) static light scattering signals of the solutions of different precursors (**TPD-2p**, **TPD-1p** and **fTPD-2p**, **fTPD-1p**) before and after ALP treatment. [precursor] = 500 μM, pH 7.4, [ALP] = 1 U mL^{-1}, in PBS buffer. The scale bar is 100 nm.

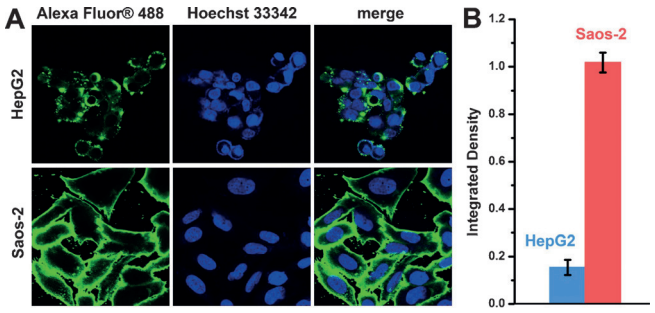

Figure 3. A) Confocal microscopy images of HepG2 and Saos-2 cells after ALPL antibody staining. Nuclei are stained by Hoechst 33342. B) Fluorescence quantification of ALPL antibody staining of HepG2 and Saos-2. The values are normalized so that of Saos-2 equals to 1.

to form a solid hydrogel (1.5 h) than **TPD-1p** does (0.5 h) (0.5 wt%). **fTPD-2p** (or **fTPD-1p**) exhibits similar behavior as **TPD-2p** (or **TPD-1p**) (Figure 2A), except that replacing the Nap motif by NBD group slightly decreases the self-assembly ability. TEM images reveal similar nanofibrils ($d = 4 \pm 2$ nm) in their solutions after ALP treatment. Static light scattering (SLS) signals of the solutions of different precursors before and after the addition of ALP confirm that all the four small molecules hardly self-assemble before enzymatic dephosphorylation, but form aggregates/nanofibrils after ALP treatment, because the signals of the solutions of precursors are almost the same with that of PBS buffer and dramatically increase after the addition of ALP.

Despite that Western blot[13] indicates a significantly higher ALPL expression in Saos-2, it represents the enzyme amount in cell lysate, mainly from the cytosol. We thus use antibody staining to confirm the different ALPL levels on the membranes of HepG2 and Saos-2 cells. According to the results in Figure 3, Saos-2 cells, indeed, express extremely high level of ALPL, as the whole cell membrane emits bright green fluorescence visualized by confocal fluorescence microscopy. Fluorescence quantification of the antibody staining indicates at least 5 times more ALPL on Saos-2 cell membrane than HepG2 cells. The expression level of ALPLs on HepG2 cell surface is moderate, compared with that of Saos-2 cells. This result justifies our choices of HepG2 and Saos-2 cells for proving the concept outlined in Scheme 1.

To verify that **TPD-2p** amplifies the difference of the ALP expression levels in different cell lines for targeting cancer cells, we use **TPD-2p** to treat HepG2 and Saos-2 cells, and use **TPD-1p** as a control. After treating HepG2 and Saos-2 cells with **TPD-2p** or **TPD-1p** at different concentrations, the cell viabilities at different time (i.e., 24, 48, and 72 hr) (Figure 4 and Figure S3) show that **TPD-2p** and **TPD-1p** exhibit similar cytotoxicity on Saos-2 cell, with the 48hr-IC_{50} values of 130, 150 μM, respectively, but **TPD-2p** is less cytotoxic than **TPD-1p** on HepG2 cells (with the 48hr-IC_{50} value of 300, 180 μM, respectively). More specifically, as shown in Figure 4A, by adding a second phosphate on the molecule of **TPD-1p** to obtain **TPD-2p**, we successfully enhance the selectivity for targeting Saos-2 cells over HepG2 cells, from 30% cell viability difference to 48% cell viability difference, 1.6-fold enhancement, at the concentration of 200 μM, and 1.56, 1.82, 1.90 fold enhancement at the concentration of 300, 400, 500 μM, respectively.

The above results agree with the significantly higher ALPL expression on Saos-2 cells (Figure 3) and support the concept illustrated in Scheme 1. That is, the dephosphorylation of **TPD-1p** generates **TPD** for immediate self-assembly, but the dephosphorylation of **TPD-2p** first results in intermediates (**TPD-1p** and **TPD-1p′**, SI), which are more soluble and diffuse more freely than **TPD**, before the second dephosphorylation to form **TPD**. High ALPL level on Saos-2 cells warrants rapidly dephosphorylate **TPD-2p** to **TPD** before the intermediates diffuse away. So **TPD-2p** and **TDP-1p** exhibit almost same inhibitory activities to Saos-2 cells. However, in the case of less ALPL on HepG2, dephosphorylation of **TPD-1p** forms **TPD** that self-assembles immediately to result in the nanofibrils on cell surface to cause cell death, but dephosphorylation the **TPD-2p** firstly generates the intermediates (**TPD-1p** and **TPD-1p′**) (Figure S4), which can drift away due to their good solubility before continuously

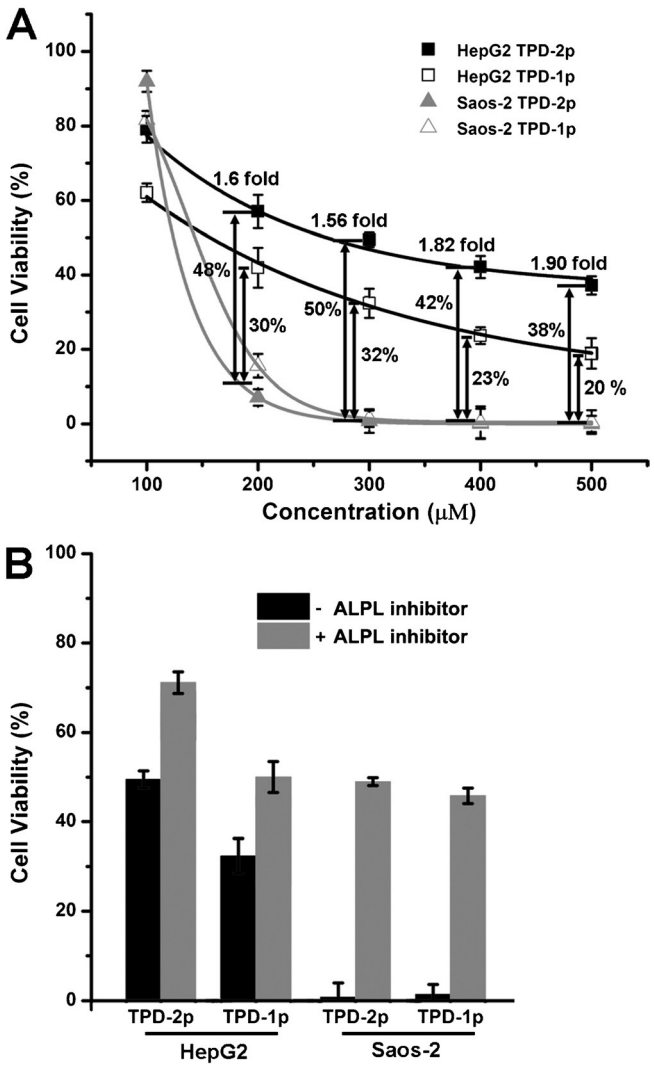

Figure 4. A) 48-hour cytotoxicity of **TPD-2p** and **TPD-1p** on HepG2 and Saos-2 cells at different concentration. The viability differences between the two cell lines are labelled as well. B) 48-hour cell viability of HepG2 and Saos-2 cells incubated with **TPD-2p** and **TPD-1p** (300 μM) with or without ALPL inhibitors (**DQB**, 2 μM) for 48 h. The initial cell number is 1×10^4 cells/well.

interacting with ALPL to lose another phosphate and then self-assemble. So **TPD-2p** is more cell compatible than **TDP-1p**.

To further confirm the ALPL-catalyzed dephosphorylation is responsible for the observed cell inhibition, we incubate HepG2 and Saos-2 cell by **TPD-2p** and **TPD-1p** together with ALPL inhibitor[14] (2,5-dimethoxy-*N*-(quinolin-3-yl)benzenesulfonamide, denoted as **DQB** and at 2 μM). As shown in Figure 4B and Figure S3, the presence of ALPL inhibitor, **DQB**, significantly reduces the inhibition of Saos-2 and HepG2 cells. Obviously, **DQB** rescues more Saos-2 cells than HepG2 cells (e.g., 50% vs. 20%) for both **TPD-2p** and **TPD-1p**. These results not only validate the critical role of ALPLs for instructing the self-assembly of small D-peptide derivatives to inhibit cancer cells, but also agree with the different ALPL expression levels on Saos2 and HepG2 cells.

The replacement of N-terminal-capped motifs results in reduced self-assembly ability and reduced cytotoxicity (Figure S5), but still allows their corresponding self-assembling molecules **fTPD** to self-assemble and form nanofibrils in pericellular space of cells. According to Figure 5, treating

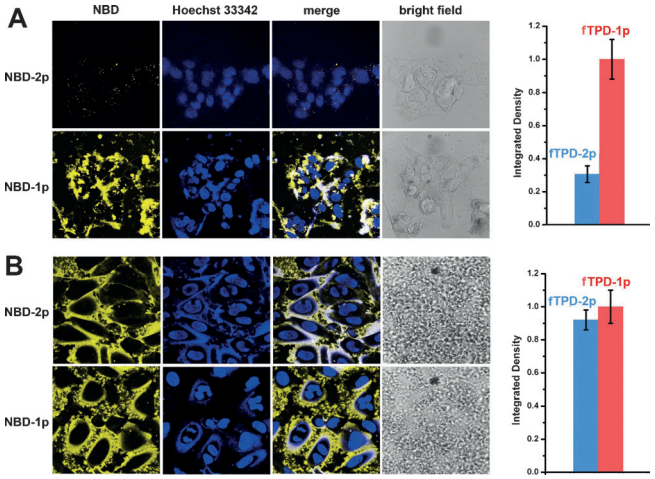

Figure 5. Confocal microscopy images and the corresponding fluorescence quantification of A) HepG2 and B) Saos-2 cells treated with **fTPD-2p** and **fTPD-1p** at the concentration of 500 μM for 12 hours. Nuclei are stained by Hoechst 33342.

HepG2 cells with **fTPD-2p** (500 μM) for 12 hours only leads to faint yellow fluorescence in the cells, likely due to endocytosis, while the addition of **fTPD-1p** into HepG2 cell culture results in strong fluorescence on the surface of the cells. Contrasting to the case of HepG2 cells, the addition of **fTPD-2p** or **fTPD-1p** in Saos-2 cell culture leads to the similar result—significant fluorescence on cell surface (Figure 5), which is more fluorescent than that on HepG2 cell treated by **fTPD-1p**. Because NBD-modified peptides fluoresce intensely in self-assembled nanofibrils,[4e] the yellow fluorescence reflects the amount of nanofibrils formed by EISA of **fTPD-2p** or **fTPD-1p**. Quantification of the yellow fluorescence in pericellular space of HepG2 and Saos-2 cells treated by **fTPD-1p** and **fTPD-2p** is highly consistent with cell viability results, which is also supported by antibody staining of ALPL. Moreover, treating the Saos-2 and HepG2 cells with **fTPD-2p** or **fTPD-1p** together with ALPL inhibitor **DQB** (10 μM) for 4 hours prior to imaging, we observe obvious difference between the cells with and without **DQB** even by naked eyes (Figure S6). Confocal fluorescence images further confirm the inhibitory effect (Figure S7). These results indicate that ALPL catalysed self-assembly to generate the strong fluorescence, agreeing with the cell viability data discussed above.

The direct measurement of the formation rate of the self-assembling molecules in a cell-based assay (SI) provides more accurate assessment of the cell targeting capability of self-assembly. Specifically, we treat the solution of **TPD-2p** and **TPD-1p** (500 μM in PBS buffer, pH 7.4) with the cell lysate of HepG2 or Saos-2 ($\approx$500 μg total protein) and examine the amount (%) of each component at different time points by

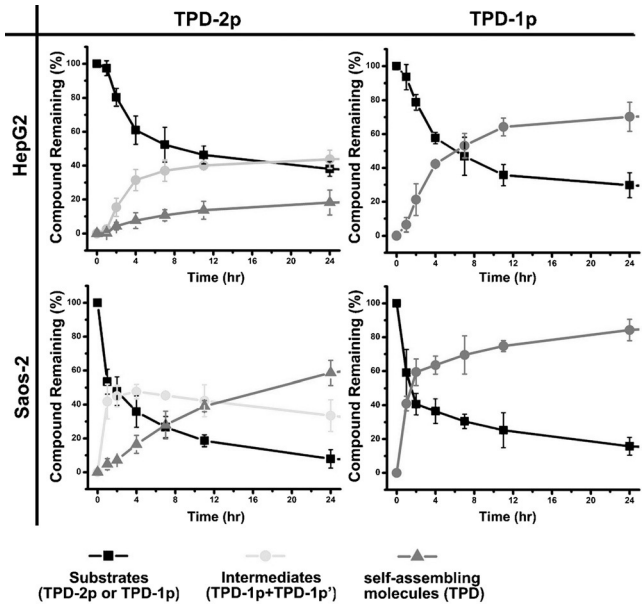

Figure 6. The time-dependent curves for dephosphorylation process of **TPD-2p** and **TPD-1p** (500 μM) after incubation with the cell lysate of HepG2 and Saos-2 at 37 °C in PBS buffer.

analytical HPLC. As shown in Figure 6 and Figure S8, in the first hour, the lysates of Saos-2 and HepG2, respectively, dephosphorylate more than 40 % and less than 5 % of **TPD-1p**. The conversion of **TPD-2p** follows the similar trend as that of **TPD-1p**. Moreover, Saos-2 lysate dephosphorylates 50 % of **TPD-2p** or **TPD-1p** within 2 hours, while HepG2 lysate takes more than 15 hours to consume half of **TPD-2p** and more than 6 hours to dephosphorylate half of **TPD-1p**. This significant difference, agreeing with the antibody staining, further supports the cell viability data and fluorescence imaging. Besides the cell-based assay, we examined the preference of ALP to the two tyrosine phosphates of **TPD-2p** in PBS buffer with commercially available ALP, and found that ALP exhibits little preference to the terminal or mid tyrosine phosphates in **TPD-2p** (Figure S9).

In conclusion, this work demonstrates a simple strategy to regulate the rate of molecular self-assembly of the enzyme reaction product by tailoring the number of phosphates on peptidic substrates. Our results verify the feasibility to achieve better target selectivity by using the self-assembling rate to amplify the difference in enzyme expressions on different cells/tissues and using molecular engineering to reduce side effects. For example, comparing to **TPD-1p**, **TDP-2p** would be a better choice for targeting osteosarcoma (e.g., Saos-2) by intravenous injection because **TPD-2p** would be more likely than **TPD-1p** to pass by liver (i.e. hepatocytes like HepG2), which expresses ALPL, to finally reach the tumor site (e.g., Saos-2) (Scheme 1). Although this work focuses on the same isoenzyme, the principle established would be applicable to different isoenzymes that exhibit different reactivity, which promises a new way for controlling dosage in precision medicine.

Acknowledgements

This work was partially supported by NIH (R01CA142746) and NSF (MRSEC 1420382). We thank Brandeis EM and Optical Imaging facilities for TEM. J.Z. is a HHMI international student fellow.

Keywords: cancer · enzymes · rate regulation · selective inhibition · self-assembly

How to cite: *Angew. Chem. Int. Ed.* **2016**, *55*, 5770–5775
Angew. Chem. **2016**, *128*, 5864–5869

[1] a) D. Hanahan, R. A. Weinberg, *Cell* **2000**, *100*, 57–70; b) D. Hanahan, R. A. Weinberg, *Cell* **2011**, *144*, 646–674.
[2] J. Zhou, B. Xu, *Bioconjugate Chem.* **2015**, *26*, 987–999.
[3] a) M. Yamanaka, N. Haraya, S. Yamamichi, *Chem. Asian J.* **2011**, *6*, 1022–1025; b) L. A. Estroff, A. D. Hamilton, *Chem. Rev.* **2004**, *104*, 1201–1217; c) T. Noguchi, B. Roy, D. Yoshihara, Y. Tsuchiya, T. Yamamoto, S. Shinkai, *Chem. Sci.* **2015**, *6*, 3863–3867.
[4] a) Z. M. Yang, K. M. Xu, Z. F. Guo, Z. H. Guo, B. Xu, *Adv. Mater.* **2007**, *19*, 3152–3156; b) J. Li, Y. Kuang, J. Shi, J. Zhou, J. E. Medina, R. Zhou, D. Yuan, C. Yang, H. Wang, Z. Yang, J. Liu, D. M. Dinulescu, B. Xu, *Angew. Chem. Int. Ed.* **2015**, *54*, 13307–13311; *Angew. Chem.* **2015**, *127*, 13505–13509; c) Y. Kuang, J. Shi, J. Li, D. Yuan, K. A. Alberti, Q. Xu, B. Xu, *Angew. Chem. Int. Ed.* **2014**, *53*, 8104–8107; *Angew. Chem.* **2014**, *126*, 8242–8245; d) J. Shi, X. Du, D. Yuan, J. Zhou, N. Zhou, Y. Huang, B. Xu, *Biomacromolecules* **2014**, *15*, 3559–3568; e) J. Zhou, X. Du, J. Li, N. Yamagata, B. Xu, *J. Am. Chem. Soc.* **2015**, *137*, 10040–10043.
[5] a) Z. Yang, H. Gu, D. Fu, P. Gao, J. K. Lam, B. Xu, *Adv. Mater.* **2004**, *16*, 1440–1444; b) S. Toledano, R. J. Williams, V. Jayawarna, R. V. Ulijn, *J. Am. Chem. Soc.* **2006**, *128*, 1070–1071; c) Z. Yang, G. Liang, B. Xu, *Acc. Chem. Res.* **2008**, *41*, 315–326; d) X. Miao, W. Cao, W. Zheng, J. Wang, X. Zhang, J. Gao, C. Yang, D. Kong, H. Xu, L. Wang, Z. Yang, *Angew. Chem. Int. Ed.* **2013**, *52*, 7781–7785; *Angew. Chem.* **2013**, *125*, 7935–7939; e) M. Zelzer, S. J. Todd, A. R. Hirst, T. O. McDonald, R. V. Ulijn, *Biomater. Sci.* **2013**, *1*, 11–39; f) A. G. Cheetham, D. Keith, P. Zhang, R. Lin, H. Su, H. Cui, *Curr. Cancer Drug Targets*, **2015**, *16*, 1–20; g) L. Cui, D. Tokarz, R. Cisek, K. K. Ng, F. Wang, J. Chen, V. Barzda, G. Zheng, *Angew. Chem. Int. Ed.* **2015**, *54*, 13928–13932; *Angew. Chem.* **2015**, *127*, 14134–14138.
[6] R. A. Pires, Y. M. Abul-Haija, D. S. Costa, R. Novoa-Carballal, R. L. Reis, R. V. Ulijn, I. Pashkuleva, *J. Am. Chem. Soc.* **2015**, *137*, 576–579.
[7] X. Du, J. Zhou, L. Wu, S. Sun, B. Xu, *Bioconjugate Chem.* **2014**, *25*, 2129–2133.
[8] M. A. T. Blaskovich, *Curr. Med. Chem.* **2009**, *16*, 2095–2176.
[9] J. L. Millan, *Mammalian Alkaline Phosphatases: From Biology to Applications in Medicine and Biotechnology*, Wiley-VCH, Weinheim, **2006**.
[10] a) W. H. Fishman, N. R. Inglis, S. Green, C. L. Anstiss, N. K. Gosh, A. E. Reif, R. Rustigian, M. J. Krant, L. L. Stolbach, *Nature* **1968**, *219*, 697–699; b) M. Uhlen, L. Fagerberg, B. M. Hallstroem, C. Lindskog, P. Oksvold, A. Mardinoglu, A. Sivertsson, C. Kampf, E. Sjoestedt, A. Asplund, I. Olsson, K. Edlund, E. Lundberg, S. Navani, C. A.-K. Szigyarto, J. Odeberg, D. Djureinovic, J. O. Takanen, S. Hober, T. Alm, P.-H. Edqvist, H. Berling, H. Tegel, J. Mulder, J. Rockberg, P. Nilsson, J. M. Schwenk, M. Hamsten, K. von Feilitzen, M. Forsberg, L. Persson, F. Johansson, M. Zwahlen, G. von Heijne, J. Nielsen, F. Ponten, *Science* **2015**, *347*, 1260419.

[11] E. G. Schuetz, J. D. Schuetz, S. C. Strom, M. T. Thompson, R. A. Fisher, D. T. Molowa, D. Li, P. S. Guzelian, *Hepatology* **1993**, *18*, 1254 – 1262.
[12] *Fmoc Solid Phase Peptide Synthesis: A Practical Approach* (Eds.: W. C. Chan, P. D. White), Oxford Univ. Press, Oxford, **2000**.
[13] http://www.abcam.com/Alkaline-Phosphatase-Tissue-Non-Specific-antibody-EPR4477-ab108337-references.html.
[14] R. Dahl, E. A. Sergienko, Y. Su, Y. S. Mostofi, L. Yang, A. M. Simao, S. Narisawa, B. Brown, A. Mangravita-Novo, M. Vicchiarelli, L. H. Smith, W. C. O'Neill, J. L. Millan, N. D. P. Cosford, *J. Med. Chem.* **2009**, *52*, 6919 – 6925.

Received: January 22, 2016
Revised: March 11, 2016
Published online: April 6, 2016

